Asian Journal of Pharmaceutical Sciences 16 (2021) 419–431

Available online at www.sciencedirect.com

ScienceDirect

journal homepage: www.elsevier.com/locate/AJPS

Review

An insight into the *in vivo* imaging potential of curcumin analogues as fluorescence probes

Yu Liu[a,b], Chuang Zhang[a,c], Hao Pan[a,c], Li Li[a,b], Yanjie Yu[a,d], Bingmi Liu[a,b,*]

[a] School of Pharmaceutical Sciences, Liaoning University, Shenyang 110036, China
[b] Judicial Identification Center of Liaoning university, Shenyang 110036, China
[c] Liaoning Key Laboratory of New Drug Research & Development, Shenyang 110036, China
[d] Liaoning Pharmaceutical Engineering Research Center for Natural Medicine, Shenyang 110036, China

ARTICLE INFO

Article history:
Received 27 July 2020
Revised 17 October 2020
Accepted 27 November 2020
Available online 5 December 2020

Keywords:
Curcumin
Fluorescent probe
Fluorescence characteristics
Structural feature

ABSTRACT

Curcumin and its derivatives have good electrical and optical properties due to the highly symmetric structure of delocalized π electrons. Apart from that, curcumin and its derivatives can interact with numerous molecular targets, thereby exerting less side effects on human body. The fluorescence emission wavelength and fluorescence intensity of curcumin can be enhanced by modifying its π-conjugated system and ß-diketone structure. Some curcumin-based fluorescent probes have been utilized to detect soluble/insoluble amyloid-ß protein, intracranial reactive oxygen species, cysteine, cancer cells, etc. Based on the binding characteristics of curcumin-based fluorescent probes with various target molecules, the factors affecting the fluorescence intensity and emission wavelength of the probes are analyzed, in order to obtain a curcumin probe with higher sensitivity and selectivity. Such an approach will be greatly applicable to *in vivo* fluorescence imaging.

1. Introduction

Conventional organic fluorescent dyes/probes, such as carboxytetramethylrhodamine (TRAMA), fluorescein, 5-carboxyfluorescein (FAM), Cy3, Cy5, fluorescein isothiocyanate (FITC) and Rhodamine B, are widely used for bioimaging applications [1,2]. However, there are still some drawbacks hampering their application in the bioimaging, including low fluorescence intensity, low photostability and insufficient stability [2,3]. Numerous studies on bioimaging and protein determination have shown that curcumin-based fluorescent probe is a promising application prospect *in vivo*, not limited to the identification of the drug itself. Curcumin-based fluorescent probes can overcome the shortcomings of organic fluorescent dyes, such as poor lipophilicity, poor photostability and low quantum yield, as well as display high sensitivity and molecular target ability that avoid possible interference of other substances with similar structure [2,4]. The emission wavelength of fluorescent probe is located in the near-infrared

* Corresponding author.
E-mail address: liubingmi@126.com (B. Liu).
Peer review under responsibility of Shenyang Pharmaceutical University.

https://doi.org/10.1016/j.ajps.2020.11.003

region, which can reduce the interference of autologous luminescence in living tissue; Excellent blood stability contributes to a reasonable metabolic rate; The fluorescence properties (*i.e.*, fluorescence lifetime, fluorescence intensity, quantum yield and emission wavelength) are significantly altered upon binding to target. These unique properties are prerequisites for *in vivo* fluorescent bioimaging.

Curcumin, a yellow polyphenolic compound, is one of the major ingredients of turmeric (*Curcuma longa* L.). It possesses a broad range of pharmacological and biological activities, such as anticarcinogenic and antioxidant activities, with good safety for human use [5]. The pleiotropic activities attributed to curcumin are considered to be closely related to its chemical structure functionalities: (i) the α,ß-unsaturated ß-diketone moiety; (ii) the 3-OCH3 and 4-OH groups on terminal phenyl; (iii) the central methylene hydrogens; and (iv) two hydrophobic phenyl domains that are jointed by a flexible linker. The presence of these functional groups endows curcumin with numerous possibilities to interact with its target proteins.

The unique properties of curcumin enhance its capability to act on various signaling pathways, including growth factor receptors, inflammatory cytokines, transcription factors, enzyme, kinases, adhesion molecules, etc. [6,7]. Curcumin plays a significant role in the prevention of human disease prevention by modulating several biological processes. Besides, it can be used to effectively scavenge both reactive oxygen and nitrogen species (ROS and RNS) [8]. In addition, curcumin and its derivatives can form complexes with iron-copper and boron in plasma due to the molecular structure of ß-diketone [9,10]. This enables them to be successfully applied for constructing small molecule fluorescent probe. TwJo benzene rings at the terminal of curcumin molecule are connected by heptadiene with seven-carbon chain, containing α,ß-unsaturated ß-diketone structure that exhibits keto-enol tautomerism (Fig. 1), which in turn results in a large delocalized π-conjugated system and rigid planar structure. Furthermore, curcumin has excellent optical properties. The short absorption wavelengths (ranging from 410 to 430 nm), inability to image in the near-infrared region, as well as poor chemical- and photo-stability (fast decomposition at pH $\geq$7 and severe fading upon photoillumination) have limited their further applications as a fluorescent dye *in vivo* imaging probes [3,11]. At present, curcumin-based probes with outstanding imaging properties for *in vivo* imaging have been successfully obtained by modifying the curcumin structure in order to improve both optical and *in vivo* dynamic properties [11–16]. These probes have been extensively used in the research of biomolecular marker, enzyme analysis, environmental monitoring, clinical examination, disease diagnosis, etc. [17,18]. In this review, the research progress and application prospect of curcumin probes are summarized, particularly in the field of fluorescence imaging.

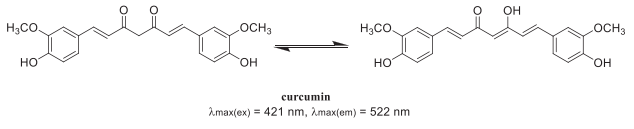

Fig. 1 – The keto-enlo tautomeric structure of curcumin.

2. Curcumin-based fluorescent probes for different biological targets

2.1. *Determination of insoluble amyloid-ß plaques*

Amyloid-ß (Aß) peptide cascade hypothesis suggests that the etiology of Alzheimer's disease (AD) may be attributed to the formation of insoluble Aß plaques in AD brain [19,20]. Aß is normally expressed in brain tissue, and its high level can be found in patients with sporadic AD. The production and clearance of Aß maintain a dynamic balance and no accumulation occurs under normal conditions. However, under pathological conditions, the balance of Aß production and clearance is dysregulated, and the excessively accumulated Aß monomer gradually forms soluble dimers and oligomers. The dimers and oligomers are cross-linked to form insoluble fibrils and fibers, which subsequently deposit into the plaques at neuronal surface and induce cytotoxicity, resulting in the decreased function of neuron cells or even die out. Therefore, insoluble Aß plaque is regarded as an early pathologic marker for the development of AD [21].

Previous studies have revealed that curcumin is able to eliminate insoluble Aß plaques and bind to amyloid deposits [22,23], which represents a small fluorescent compound that can cross the blood-brain barrier (BBB) and detect Aß plaques in APPswe/PS1dE9 mouse mode. Curcumin has been employed for positron emission computed tomography (PET) imaging studies because it can be labeled with the radioactive isotope fluoro-18 [24]. However, some disadvantages, such as high detection cost, time-consuming process and radiation hazards of PET scan, have limited its application in the clinic. Near-infrared fluorescence (NIRF) probes have been recently harnessed for *in vivo* imaging due to its characteristics of non-invasive, safe, low-cost, fast, great penetration depth and low interference from autologous luminescence in living tissue. Although many cyanine dyes and their derivatives have been established, including the commercially available NIRF probes, the large molecular weight and electrical charge have limited their ability to penetrate the BBB, making them unsuitable for labeling the in-brain Aß plaques [25]. In principle, NIRF probe for the in-brain imaging of Aß plaques must have the following basic properties: (i) high affinity and specificity to Aß plaques (inhibition constant Ki $<$ 20 nmol/l); (ii) emission wavelength of NIRF (650 — 900 nm); (iii) strong BBB penetration and rapid clearance in brain tissue (reasonable lipophilicity: logP between 2 and 3.5, molecular mass $<$600 Da); (iv) high quantum yield with a large Stokes shift; (v) reasonable stability in blood; and (vi) different fluorescence properties that are significantly altered upon binding to Aß plaques [26]. Mounting evidence indicates that the retina, an optic nerve originate as a developmental outgrowth of the forebrain, is also profoundly affected by AD. To visualize retinal Aß pathology *in vivo*, Koronyo and co-workers have previously developed a noninvasive retinal amyloid imaging method for rodent ADtg models, using curcumin as a contrast agent. This approach enables

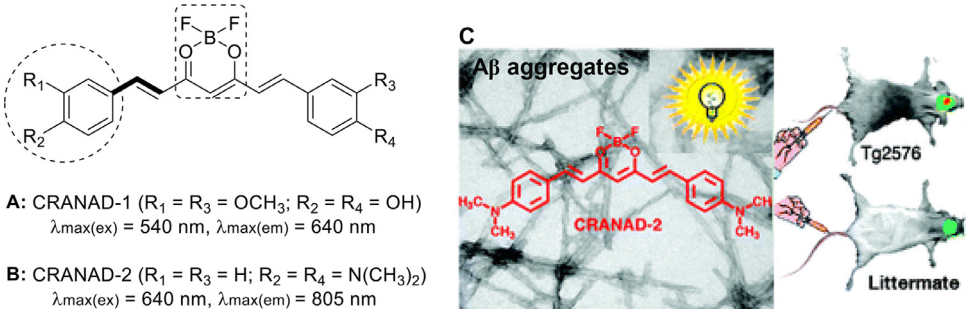

Fig. 2 – CRANAD probes for detecting insAß aggregates: (A,B) CRANAD-1 and CRANAD-2. Dotted circles, dotted boxes and bold lines denote donors, acceptors and π–bridges, respectively. (C) Specific binding and labeling of CRANAD-2 to Aß plaque *in vivo* (Reproduced with permission from [26]. Copyright 2020 Canadian Science Publishing.).

noninvasive detection and real-time monitoring of individual retinal Aß deposits in live ADtg mice [27]. Fluorescent imaging data demonstrate the successful colabeling of curcumin with various anti-Aß mAbs for the detection of multiple intracellular and extracellular deposits across retinal layers in AD patients [27].

Although curcumin has a high-affinity binding with insoluble Aß plaques, it is not suitable for NIRF imaging, probably due to its shorter emission wavelengths, limited BBB penetration, and fast metabolic rate [18,28]. CRANAD-1 is a curcumin analogue that can be acquired by introducing difluoroboron ring onto the ß-diketone structure of the curcumin molecule (Fig. 2A). Benzene ring, with an electron-donating substituent and electron-withdrawing boron difluoride as electron donor and electron acceptor, respectively, formed a donor-π-acceptor (D-π-A) conjugated system by connecting with seven carbon chain olefins (Fig. 2C), which can reduce the HOMO-LUMO energy band gap. Therefore, both maximum excitation wavelength and emission wavelength of CRANAD-1 fluorescence were significantly redshifted compared to those of curcumin. Moreover, CRANAD-1 has been reported as a protease inhibitor of HIV-1 and HIV-2 [29], and Anna Moore's team found that this compound could target insoluble Aß plaques near the NIR region [26]. To further redshift the emission wavelength towards the near-infrared spectrum range, the research group [26] substituted the phenolic hydroxyl group on the CRANAD-1 with more powerful electron-rich donor N,N′-dimethyl group, and innovatively obtained a novel NIRF probe compound CRANAD-2 with high BBB penetration (Fig. 2B). The fluorescence properties of CRANAD-2 were significantly altered upon mixing with insoluble Aß plaques, example, a remarkable increase (70-fold) in fluorescence intensity, a significant 90 nm blueshift (805–715 nm), and a high (nearly 70-fold) quantum yield (0.006–0.40). Furthermore, the probe demonstrated a high affinity (Kd = 38.0 nmol/l) to Aß plaques and considerable serum stability. CRANAD-2 could achieve specific binding and NIRF labeling to the in-brain Aß plaques of mice within 30 min. This is supported by *in vivo* imaging experiments performed on the brain tissue sections of transgenic 19-month-old Tg2576 mice injected via tail vein (Fig. 2C). Although CRANAD-2 met almost all the basic requirements of NIRF probe for real-time live

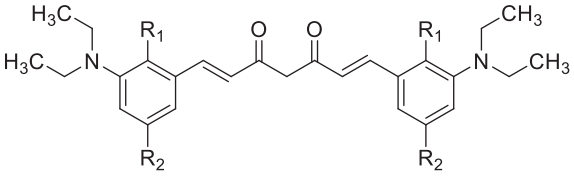

Fig. 3 – Structure of Dye 1–3.

imaging of Aß plaques, its elimination rate was significantly slower in the brain tissue of treated mice than in the blood. Compared to an Aß plaque-specific probe (Pittsburgh probe B), it entered into the brain much lesser and was eliminated more slowly.

In order to increase the emission wavelength of fluorescent probes and their binding strength to Aß plaques, Si et al. [30] designed and synthesized three curcumin-based NIR dyes (Dye 1–3) that could bind to insoluble Aß plaques (Fig. 3A–3C). The stabilities of the three dyes in aqueous solution and mouse plasma were found to be excellent. Due to the introduction of electron-rich donor groups, such as N,N-diethylamine and methoxy (-OCH3), at the terminal of the molecules, the compounds displayed large Stokes shifts (>130 nm) and their maximum fluorescence emission wavelengths were within the NIR range, which similar to the properties of NIRF imaging. The maximum emission wavelengths of Dyes 1–3 were observed to be unchanged. Due to the restriction of intramolecular rotation, the fluorescence intensity and quantum yield of Dyes 1–3 increased to different degrees after binding to Aß plaques. This may improve the probability of various decay modes of the excited state back to the ground state, significantly reduce the occurrence of non-radioactive decay reaction, and ultimately enhance

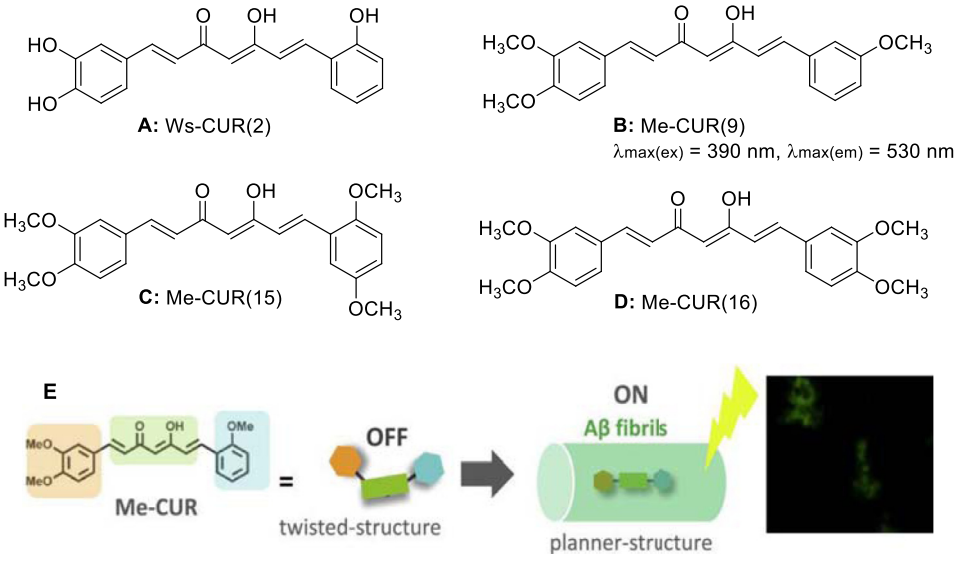

Fig. 4 – Me-CUR probes for detecting insAß fibrils: (A)Structure of Ws-CUR. (B-D) Me-CUR probes: (B) Me-CUR(9), (C) Me-CUR(15) and (D) Me-CUR(16). (E) Illustration of Me-CUR as "off-on"fluorescent probes for Aß fibrils(Reproduced with permission from [1]. Copyright 1989 Published by Elsevier Inc.).

the luminous ability of the dye molecules. The superior coplanarity and strong electron-donating capability also resulted in the high fluorescence intensity and quantum yield of Dye 2. Saturation concentration method was performed for the determination of dye affinity with Aß plaques, and the results showed that the three compounds possessed the ability to bind to insoluble Aß plaques, and Dye 2 displayed the strongest binding affinity (Kd = 1.36 μmol/l). *In vivo* imaging results showed that Dye 2 had specific combining ability to Aß plaques [30]. In that experiment, Dye 2 could detect Aß plaque sites in the brain of 17-month-old APP/PSI mice, after tail intravenous injection of the dye within 1 h, and the fluorescence intensity at the plaque sites reached its maximum at approximately 2 h after injection [30]. Efforts of the research group demonstrated that Dye 2 was increasingly accumulated in the Aß plaques, suggesting that Dye 2 molecules exhibit an aggregation-induced emission [30]. However, the study did not hold an in-depth discussion.

The structure-activity relationship based on thioflavin T fluorescence analysis [31] showed that the 3,4-site dimethoxy groups of benzene ring and the heptaatomic olefin chains containing ß-diketone were deemed as the necessary structures for the identification of insoluble Aß fibers. Sato et al. [1] synthesized a series of highly sensitive molecular rotor-type curcumin-based fluorescent probes with "off-on" property, which could be used as an effective alternative to the commercial probe thiocyanin T for the *in vitro* detection of insoluble Aß fibers. The group designed and synthesized Me-CURs compounds, inspiring by a study on the anti-Aß-aggregation and structure-activity relationships of curcumin analogues, particularly the compound Ws-CUR(2) (Fig. 4A) with obvious inhibitory effects and a high water solubility far superior to curcumin. This lead compound could reduce the inhibition of Aß-aggregation, retain the bonding with insoluble Aß fibers by substituting the hydroxyl groups on the benzene ring with -OCH3, and introduce varying amounts of -OCH3 at different positions in the benzene ring [32]. The Me-CUR compounds consisted of curcumin derivatives with symmetric and asymmetric structures and mono-double carbonyl curcumin analogues with a seven-carbon chain shortened to a three-carbon chain and a five-carbon chain between two benzene rings [13]. Among the synthesized compounds, Me-CUR(9), Me-CUR(15) and Me-CUR(16) were the most abundant (Fig. 4B–4D), and Me-CUR(9) exhibited the most significant change in fluorescence intensity. When the compound was combined with insoluble Aß fibers, the free rotation of the single bond in the benzene ring around the olefin connector is restricted, which in turn lead to a high molecular flatness. Therefore, Me-CUR(9) could be firmly bound to Aß fibers, resulting in a sharp increase in emission intensity, with an "off-on" fluorescence signal (Fig. 4E). This suggests that Me-CUR(9) may play a key role in the detection of insoluble Aß fibers. Molecular docking results showed that Me-CUR(9) and thioflavin T were combined inside Aß fibers via hydrophobic action and hydrogen bond, and the binding sites were typically the same [1].

2.2. *Detection of soluble amyloid-ß plaques*

The difficulties in AD drug development have revealed the necessity of early intervention in AD patients [33–35]. Thus, an early diagnosis of the pathophysiological hallmarks of AD is desperately needed. Mounting evidence suggests that soluble amyloid-ß beta (soluble Aß), such as dimers and oligomers, could exist during the presymptomatic stage of AD, and its neurotoxicity was significantly higher than insoluble Aß [36–39]. Thus, it is more likely to be a biomarker for the early detection of AD. Both soluble oligomers and insoluble fibers/aggregates were also found during the progression of

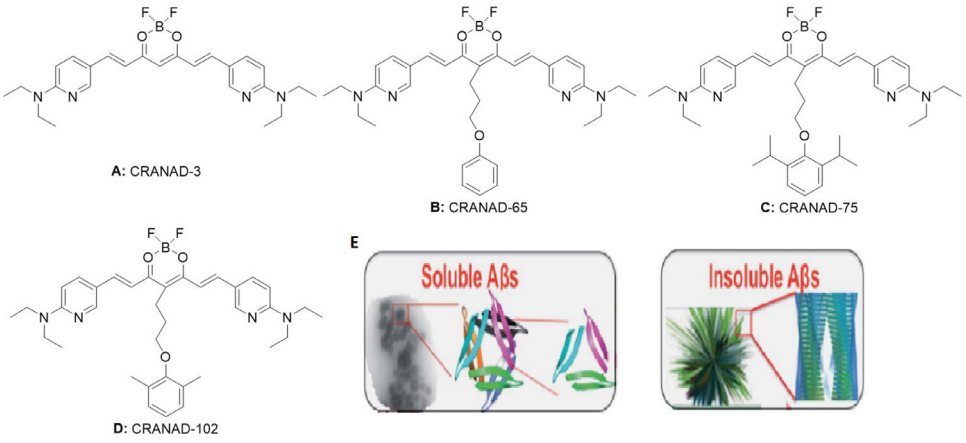

Fig. 5 – CRANAD probes for detecting sAß fibrils. (A-D)Structure of CRANAD probes: (A) CRANAD-3, (B) CRANAD-65, (C) CRANAD-75 and (D) CRANAD-102. (E) Cartoon pictures suggest that the accessibility decreases from soluble Aßs to insoluble Aßs (Reproduced with permission from [46]. Copyright 2017 The Royal Society of Chemistry.).

AD. Therefore, the development of fluorescent probes that specifically targets on soluble Aß peptides could provide a new idea for the study of curcumin probes.

Ran and co-workers [26] have designed and synthesized a list of CRANAD compounds, which are borocurcumin-containing NIRF probes with emission wavelengths ranging from 650 to 900 nm, through the redshift modification of curcumin. However, differentiating between soluble and insoluble Aßs with a small molecular probe is extremely challenging. The variations in the secondary and tertiary structures of soluble and insoluble Aßs may lead to differential binding affinities for anti-Aß antibodies, although the two forms of Aßs contain the same polypeptide chain [40,41]. Small molecule probes can be modified to distinguish between soluble and insoluble Aßs based on their structural differences. Non-planar "T-Shape" curcumin analogues has been used to differentiate soluble and insoluble Aßs, since the planar portion of the curcumin can incorporate into the ß-sheet structure of Aß species, which eventually improves the fluorescence intensities of soluble and insoluble Aß [26,42–45]. Li et al. [46] designed a non-planar "T-Shape" curcumin analogue, where the planar moiety could be inserted into the ß-sheet, thus adjusting the accessibility and selectivity of the probe to soluble Aß (Fig. 5E). In addition, the curcumin scaffold can be tuned by changing the stereo-hindrance to CRANAD-75 > −102 > −65 > −3 [46].

Among the designed compounds, CRANAD-3 (Fig. 5A) has sensitive responses to both soluble Aß and insoluble Aß [27,43–45], which is not selective for soluble Aß. CRANAD-65 responded significantly to Aß42 oligomers and Aß40 dimers. This may be due to the fact that the curcumin scaffold with phenyloxy alkyl chain at the 4-position displays a high hydrophobicity and can non-specifically bind to the serum, thus leading to a particular selectivity towards soluble Aß. CRANAD-65 (Fig. 5B) displayed a significant selectivity at the initial incubation period ($t = 0$ min); but reduced greatly with increasing incubation times ($t = 0$–15 min), probably due to the low steric hindrance of the phenyl ring at the 4-position. To further increase the steric hindrance, the group evaluated different types of CRANAD, and found that CRANAD-75 (Fig. 5C) exhibited a good selectivity (88.5-fold) towards monomeric Aßs. As opposed to CRANAD-65, its selectivity remained stable with increasing incubation times, probably due to the existence of two isopropyl groups on the phenyl ring of CRANAD-75. Moreover, CRANAD-75 did not respond significantly to oligomeric Aßs, indicating that the steric hindrance of the two isopropyl groups is quite bulky to prevent it from being engaged in the ß sheet structure of the oligomers. Therefore, it is necessary to decrease the hindrance in order to enhance the selectivity of CRANAD-75 towards oligomeric Aßs. By substituting two isopropyl groups in CRANAD-75 with two methyl groups, CRANAD-102 (Fig. 5D) could respond better to oligomeric Aßs, with a 4.33-fold increase in its binding affinity. In addition, CRANAD-102 exhibited a 68-fold higher affinity towards soluble Aß (7.5 ± 10 nM) than insoluble Aß (505.9 ± 275.9 nM), which could penetrate the BBB more rapidly and had certain stability in serum. The imaging data revealed that CRANAD-102 could be applied to detect soluble Aß *in vivo* using 4-month-old APP/PS1 transgenic mice. Li et al. [46] also demonstrated that the levels of soluble Aß could be monitored by CRANAD-102 from 4 to 12 months of age. Altogether, these findings indicate that a decrease in steric hindrance could improve the accessibility/tightness of different Aß species, and thus allow us to distinguish between soluble and insoluble Aß species. Furthermore, CRANAD-102 was highly selective for soluble Aß over other aggregation-prone proteins/peptides (*e.g.* amylin, α-synuclein and tau) [46]. Moreover, Yang et al. demonstrated that NIRF ocular imaging (NIRFOI) with CRANAD-102 could be used to monitor the therapeutic effects of AD inhibitor [47]. The results showed that CRANAD-102 reached NIRF signal peak around 60 min, and the difference at this time point was about 3.14-fold, while the dynamic level of CRANAD-102 in 4-month-old APP/PS1 mice was different from that in 14-month-old APP/PS1 mice, where the peak shifted to 30 min. This indicates that old mice have large Aß oligomers that can hold CRANAD-102 longer. Furthermore, the data of CRANAD-2 and CRANAD-102 are complementary to each other, probably

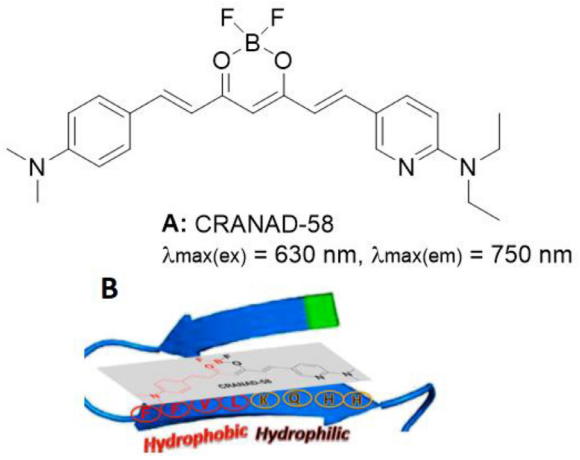

Fig. 6 – CRANAD probes for detecting sAß fibrils: (A) Structure of CRANAD-58. (B) The proposed interaction model between CRANAD-58 and Aß (Reproduced with permission from [44]. Copyright 2002 The American Association for the Advancement of Science.).

due to their differential substrate specificities. For example, CRANAD-2 is more specific to insoluble Aß species; while CRANAD-102 is more specific to soluble Aß species [47].

There are two main hydrophobic sites (Site A and B) inside Aß fibrils. Site A consists of hydrophobic amino acid residues along the long axis of the fibrils, while Site B has the core fragment (KLVFF) of an Aß40/42 peptide [48]. At a structural level, Site A possesses higher steric hindrance compared to Site B. CRANAD-2 could be used as an excellent probe for the detection of insoluble Aß aggregates because its fluorescence properties alter significantly following the reaction, such as emission blue shift, fluorescence intensity increase, quantum yield increase, and response time decrease [28]. The reason for this may be that the aromatic ring of CRANAD-2 is extended after binding to Site A, and the binding to the hydrophobic site can result in a specific hydrophobic interaction [45], which in turn enhances the fluorescence effect. However, CRANAD-2 is not capable to detect soluble Aß, and no significant changes in fluorescence properties were observed after its incubation with soluble Aß species. The interaction between Site B of monomeric Aß40 and CRANAD-2 was most likely weak. Such weak interaction could be partly explained by the unmatched structure of CRANAD-2 as well as the hydrophilic (HHQK) and hydrophobic (LVFF) segments of Site B. Consequently, Zhang et al. [45] designed and synthesized an asymmetric curcumin analogue, CRANAD-58 (Fig. 6A), that could bind to the hydrophobic fragment LVFF [49], Besides, the nitrogen of the pyridyl ring could interact with the hydrophilic fragment (HHQK) of Aß40/42 peptide to form hydrogen bonds (Fig. 6B) with high binding strength [50]. Furthermore, the addition of pyridine ring could extend the π-conjugation, shift both emission and excitation wavelengths into NIR region, and enhance the fluorescence intensity [49,50]. As reported previously, CRANAD-58 demonstrated fluorescence excitation and emission peaks at 630 and 750 nm, respectively, and exhibited a strong binding capacity for soluble Aß, with a significant increase in fluorescence intensity (about 60-fold) and a remarkable blue shift in the emission spectrum. The in-brain fluorescence signal of APP/PS1 mice at each time point after intravenous injection of soluble Aß was significantly higher than that of age-matched wild-type mice, implying that CRANAD-58 can be applied for the *in vivo* detection of soluble Aß species. More importantly, CRANAD-58 satisfies the characteristics of excellent lipophilicity (log P), reasonable BBB penetration, etc.

2.3. *Determination of in-brain reactive oxygen species (ROS)*

Oxidative stress plays a critical role in the progression of AD. Previous studies have demonstrated that the levels of ROS are relatively higher in AD brain than in healthy brain [10,14]. Moreover, Aß plaques can grow gradually with the progression of the disease. Bacskai et al. [51] showed that the plaques could impair mitochondrial function and dysregulate Ca^{2+} homeostasis, leading to oxidative stress-induced cell apoptosis. Aß plaques are mainly classified as “active” and “inactive/silent” plaques, and such classification can explain the non-significant relationship between Aß plaque loading and AD severity [52,53]. During Aß plaque growth and formation, various ROS are produced mainly through the Fenton reaction. The generated ROS can trigger an excess accumulation of proinflammatory cytokines [54–56], thereby causing the microglial cells to aggregate around the plaques [57–59]. This may result in the extensive production of ROS and neuronal apoptosis [59]. From these findings, it can be speculated that ROS levels are elevated in the active plaques, which may serve as an indicator to distinguish between active plaques and inactive plaques.

Yang et al. [14] designed and synthesized CRANAD-61 (Fig. 7A), an oxalate-curcumin-based NIRF probe, for the *in vivo* determination of ROS levels. This probe has been used for dual-color imaging, by producing significant wavelength shift in response to oxidative stress [10]. Given that the signal changes from both channels/wavelengths are intercorrelated, the imaging data obtained from the two channels could be verified against each other. Besides, CRANAD-61 has been used to detect the relative levels of ROS in AD mouse brain and monitor the changes in ROS levels with age, as demonstrated by whole-brain NIRF imaging. Through the incorporation of oxalate as a sensing element, the curcumin-based probes were developed for fluorescence imaging in the 640–900 nm NIR window. Upon its reaction with ROS [14], the oxalate moiety was eliminated, and subsequently converted to CRANAD-5 (Fig. 7B). The conjugate structure was reduced and “quenching” occurred, resulting in a significant blue shift of excitation/emission wavelengths (<640 nm). Such changes may be applied to the dual-color microscopic image system [10], and the conversion from NIR window to non-NIR window turns the visible light into invisible light (Fig. 7C). Another important advantage of the oxalate ester moiety is its ability to extend Ex/Em, which is necessary for the deep tissue penetration of NIR light. Since the electron delocalization of ester is greater than that of fluorides, the excitation/emission wavelengths could be elongated by substituting BF2 with oxalate boron ester. It should be noted

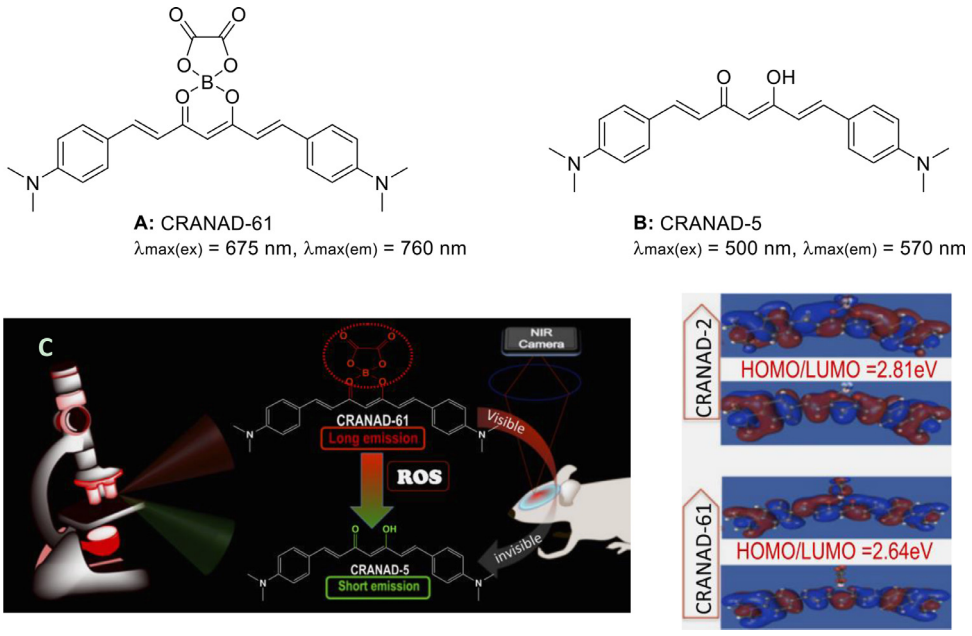

Fig. 7 – CRANAD probes for detecting ROS: (A) CRANAD-61. (B) CRANAD-5. (C) The design strategy for ROS-sensitive imaging probes, and (D) HOMO/LUMO of CRANAD-2 and CRANAD-61. The energy gap of CRANAD-61 is smaller than that of CRANAD-2 (Reproduced with permission from [14]. Copyright 2017 Published under the PNAS license.).

that the smaller the HOMO-LUMO energy gap, the greater the excitation/emission wavelengths [60], and the electron delocalization of oxalate ester could result in a smaller HOMO-LUMO energy gap in CRANAD-61 than in CRANAD-2 (Fig. 7D). During the reaction process between CRANAD-61 and ROS, the nucleophilic attack on the two carbonyl groups of oxalate is found, thus generating dioxy groups and leaving. The stronger the electrical absorption of curcumin connected with the carbonyl group, the better the leaving properties and the more conducive to the fluorescence reaction.

CRANAD-61 is a rapidly reactive imaging probe for ROS detection, and significant fluorescence changes could be observed after 1 min. More importantly, CRANAD-61 is quite sensitive to low level of ROS. Besides, CRANAD-61 has a strong capability for BBB penetration. The 14-month-old APP/PS1 mice were injected with CRANAD-61 and then imaged at various time points. The results indicated that CRANAD-61 could penetrate the BBB to label Aß plaques in the brain after a 5-min administration. This implies that CRANAD-61 is a fast response, high sensitive fluorescent probe for the *in vivo* detection of ROS activity, at both microscopic and macroscopic levels.

2.4. *Detection of cysteine (Cys) level*

As a precursor amino acid of glutathione (GSH), Cys is responsible for several important processes, such as catalysis, synthesis, binding, signal transduction, and metabolism [61–64]. Since GSH is closely related to the biological function and development of many diseases, an early detection of Cys in organisms is a matter of great importance [65–73]. However, the structures and reactivity of Cys, homocysteine (Hcy) and

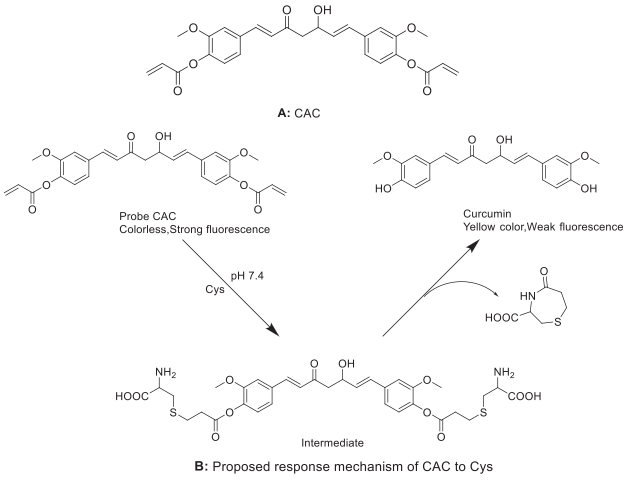

Fig. 8 – CAC probes for detecting Cys specifically: (A) Structure of CAC. (B) Proposed response mechanism of CAC to Cys.

GSH have limited the selectivity of Cys probes. In recent years, some curcumin-based fluorescent probes have been reported to selectively detect Cys [74].

Curcumin has been used as the mother molecule of probe because of its excellent biocompatibility and optical properties [75,76]. Pang et al. [74] developed a new curcumin-based colorimetric and fluorescent probe CAC for the selective detection of Cys (Fig. 8A). Upon its conjugate addition/cyclization reaction with Cys, the strong fluorescence emission of this probe was revealed by a fluorescence quenching at 490 nm, a decease in absorbance

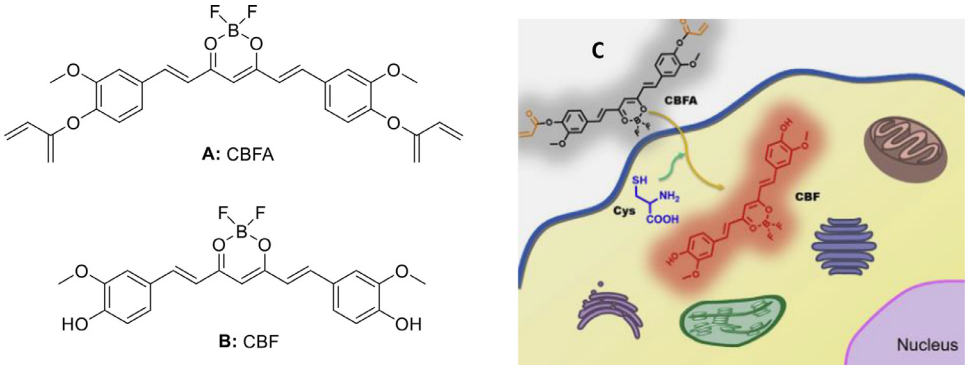

Fig. 9 – CBFA probes for detecting Cys with high selectivity: (A) CBFA. (B) CBF. (C) The recognition process of Cys in living cells by the probe CBFA (Reproduced with permission from [83]. Copyright 2019 Elsevier Ltd.).

at 400 nm, and a new peak at 427 nm, which could provide high sensitivity for living cell imaging. It is worth noting that CAC probe has good sensitivity and selectivity to Cys compared to other relevant analytes (*e.g.* GSH and Hcy). With increasing Cys concentrations (0–20 μM), the fluorescence intensities of CAC were reduced gradually, together with a decrease in fluorescent quantum yield (from 0.20 to 0.02). This indicates that the fluorescence intensity of CAC probe has a good linear correlation with Cys concentrations within the range of 0–20 μM. After mixing with Cys, CAC probe first underwent conjugate addition, and then released curcumin molecule for cyclization to generate a seven-membered ring cyclic amide (Fig. 8B) [76–80]. The excellent selectivity of CAC probe towards Cys over GSH and Hcy can be explained by the kinetic rates of the intramolecular cyclization reaction that forms a seven-membered ring (Cys) instead of eight-membered ring (Hcy) [81,82]. Moreover, the tripeptide of GSH is large in volume, which affects the internal cyclization of GSH. Therefore, CAC probe has better sensing performance than other interferences on Cys, and only shows obvious fluorescence quenching effect on Cys. Furthermore, CAC has been successfully used to determine Cys in living cells, with a good cellular and biological permeability. The change in the fluorescence intensity of CAC probe is related to the intracellular level of Cys, which offers great potential in living biological systems [74].

Curcumin difluoroboron complexes, as a typical high-performance fluorophore, is not only a probe with specific fluorescence response to *in vivo* Aß plaques, but also a cellular mercaptan bioimaging tool. Chen et al. [83] developed a novel CBFA probe with red fluorescence emission (Fig. 9A), which demonstrated a high selectivity towards Cys over GSH and Hcy. Additionally, the CBFA probe was adaptable to a broad range of pH and had a low cytotoxicity profile under various biological conditions, which could be used for the selective detection of Cys in living cancer cells. The absorption maxim of CBFA was observed at 461 nm and red-shifted to 510 nm upon the measurement of recovered fluorogen, ascribing to the absorption of the charge-transfer excited of CBF (Fig. 9B). The reaction is speculated to progress through a concerted mechanism (intramolecular Michael-type addition), as revealed by high-performance liquid chromatography and high-resolution mass spectrometer [84,85]. The two acrylate groups in CBFA probe can serve as recognition moieties connecting at their 5'-ends to a fluorogen, in order to avoid possible background interference. The rapid and selective detection of Cys (Fig. 9C) can be improved by accelerating the reaction between CBFA and Cys as well as preventing the formation of unstable 8-membered ring or much larger ring with GSH and Hcy [83].

Cys participates in the regulation of oxidative stress and plays a crucial role in mitochondrial dysfunction [86]. Thus, it is necessary to develop a specific probe for the detection of mitochondrial Cys levels in living cells. In general, low selectivity and unspecific mitochondria targeting are the two major problems encountered during the detection of mitochondrial Cys. Zhang et al. [87] successfully solved these problems by adopting the combination strategy of Michael addition and cyclization reaction to develop a mitochondrial-targetable DFB1 fluorescent probe (Fig. 10A) for the dual-channel imaging of Cys in the endogenous mitochondria of living cells. In the probe DFB1, curcumin structure acts as a NIR fluorescent group, triphenylphosphonium (TPP) cation moiety acts as a mitochondrial targeting unit, and α,ß-unsaturated ketone containing acrylate group acts as a specific functional moiety of Cys. Among them, acryloyl group and Cys are first generated into a seven-membered ring through Michael addition and cyclization reaction, and the ester bond was then cleaved to form DFB-OH (Fig. 10B). This probe had a strong fluorescence emission at 560 nm after mixing with Cys, and reached a new NIR peak at 680 nm. This can be ascribed to the weaken electron-donating ability of the phenolic group after the addition of acryloyl group into DFB1. Through the transition from DFB1 to DFB-OH, it is possible to accurately detect the levels of mitochondrial Cys. Moreover, DFB1 exhibited a greater ability to penetrate the cell-membrane in living cells. This probe also solved another issue of unspecific mitochondrial targeting. The inner membrane of mitochondria usually had a large negative membrane potential, while the triphenylphosphonium moiety in DFB1 had a positive charge, which displayed a high localization tendency towards cell mitochondria. In a nutshell, the dual-channel DFB1 fluorescent probe based on curcuminoid

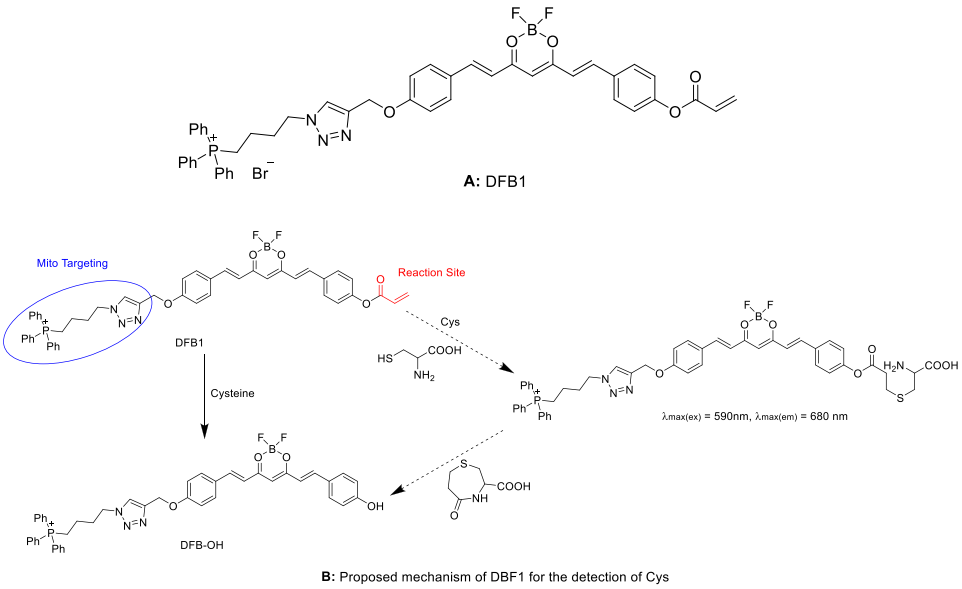

Fig. 10 – Proposed mechanism of DBF1 for the detection of Cys: (A) Structure of DBF1. (B) Proposed mechanism of DBF1 for the detection of Cys.

difluoroboron can be used to assess the mitochondrial levels of Cys in living cells, with high selectivity and good membrane permeability.

2.5. *Detection of cancer cells*

The ß-diketo-moiety of curcumin is able to form complex with a variety of metal ions, in order to achieve a higher stability. Besides, curcumin and its derivatives showed a great applicability for detecting the pathological changes in various cancer cell lines, due to its high selectivity and good bioactivity [88]. The two *N*,*N*-dimethyl substituents in the p-positions of the aromatic rings of curcumin and boron difluoride moiety at the enol-keto-group induced a strong redshift of fluorescence emission, which specifically targeted the compound in the NIR region. In addition, ammonia groups could increase the ability of curcumin to resist hydrolysis. Pröhl et al. [89] systematically altered the curcumin ligands in BF2-complexes, and synthesized novel compounds for the detection of cancer cells (Fig. 11A). To enhance solubility and π-π-stacking interactions, various electron donors were introduced into the aromatic rings, leading to the improvement of optical properties and redshift of fluorescence emission [10,90]. However, the complexes showed fairly high quantum yields and photostability. Compound 11A introduced charges to triphenylphosphane, indicating the absorption of complex 11A in the cell membrane. The fluorescence analysis of this complex revealed a strong green fluorescent signal in gastric cancer cells without significant cell toxicity. However, all BF_2-complexes showed weak fluorescence signals in phosphate-buffered saline solution due to aggregation effects.

Curcumin and its derivatives have been recognized as potential ligands for transition metals. Rare earth metal

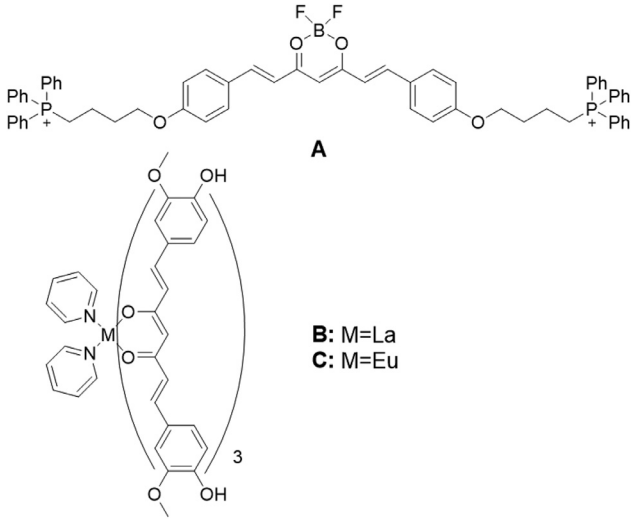

Fig. 11 – Probes for detecting cancer cells: (A) BF_2-complex. (B,C) Rare earth metal complexes.

complexes $[M(py)_2\ (CUR)_3]$ (Fig. 11B and 11C) were introduced into the curcumin molecule, and two pyridine ligands were added [90]. Increased fluorescence could be observed when compared with rare earth metal complexes in the absence of pyridine ligands, because the planar structure ensures an extension of the π-conjugated system. Obviously, the Eu complex showed photoluminescence in the NIR region, which could be activated by the pyridine ligands [89]. Additionally, both Ln complexes displayed high σ-values and non-toxicity profile, and thus are applicable for single-photon or two-photon fluorescence imaging. This indicates that both compounds have better hydrophobicity and a strong ability

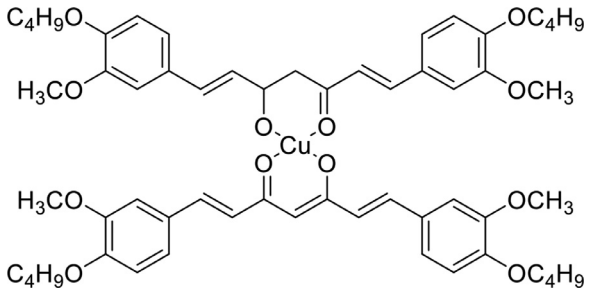

Fig. 12 – Complex probes for detecting cancer cells.

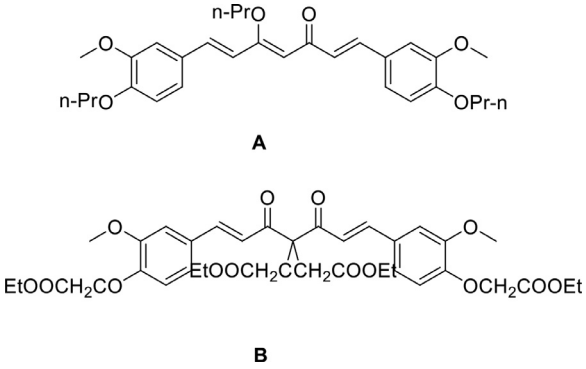

Fig. 13 – Two novel multibranched dyes curcumin-based for detecting canc.

to bind to cancer cells compared to Ni- and Zn-complexes by enhancing their localization on cell membrane.

As opposed to conventional confocal microscopy, two-photon microscopic technique offers numerous advantages, such as localized excitation, high penetration depth, prolonged observation period and early cancer detection [91–93]. The application of this technique is largely dependent on the enhancement of two-photon absorption (TPA) cross-section. The conjugation length, donor and acceptor strengths, and π-center planarity are the crucial factor for improving TPA cross-section [94,95]. Notably, square-planar complex formed by curcumin complexation with copper (II) ions exhibited larger TPA cross-section and higher quantum yields in the NIR region compared to its free ligand [89]. Pi et al. [96] characterized a novel multi-branched Cu(II) complex linked by π-conjugated ligands - CuL2-complex (Fig. 12), and about 3-fold increase in TPA cross-section (σ) was observed due to the effect of intramolecular charge transfer [89]. With regard to its diagnostic advantages, CuL2-complex exhibited moderate σ-values, optimum excitation wavelength ($\lambda = 760$ nm), a low toxicity profile even at higher concentrations or longer incubation period, and a targeted cytosolic or nuclear localization. Both *in vivo* and *in vitro* imaging studies revealed that the complex exhibited good tumor-targeting capability and high photostability, and was able to distinguish between cancerous tissue and noncancerous tissue, which could be used for early tumor diagnosis.

In vivo assessment demonstrated an increase in fluorescence intensity in cancer tissue traced back to the overexpression of epidermal growth factor receptor (EGFR). Complex 12 was able to distinguish between normal and cancerous lung tissue *in vivo*. One possible reason may be that complex 12 is a good match with EGFR antibodies. The two ethyl functionalities were introduced into the phenyl rings to form a bipolar donor-acceptor-donor (D-A-D) structure, which could be beneficial to two-photon microscope imaging, possibly due to a large π-conjugation structure and excellent co-planarity in the molecule [97,98].

Based on the investigation of one- and two-photon absorption properties, Xu et al. [99] designed and synthesized two novel multi-branched dyes based on curcumin molecules (Fig. 13A and 13B). The TPA cross-sections of dye 13a and dye 13b measured by two-photon excited fluorescence (TPEF) were 1143 and 842 GM, respectively. Moreover, these compounds exerted low cytotoxicity against MCF-7 cells. Furthermore, *in vivo* and *in vitro* analyses showed that dye 13A could enter and accumulate in the cancer cells, which makes it an ideal material for cancer cell detection.

For dye 13A, the diphenyl-carbonyl-heptantriene moiety displays the full molecule planarity, which conforms to the characteristics of the π-conjugated system. For dye 13B, the symmetry of the molecular structures has reached a quite satisfactory level. The whole molecular conformation folds around the ß-diketonate axis, but two hydrogen atoms attached to a carbon atom between the ß-diketone groups are substituted by two ethyl acetate groups, resulting in the destruction of a highly electron delocalized molecule and its dissolution into two smaller π-conjugated systems. Therefore, the fluorescence intensity of dye 13A is stronger than that of dye 13B. The stronger donor groups (such as propyl and acetate ethyl groups) and the extension of π-conjugation system are conducive to a larger TPA cross-section, which is more beneficial to visualize the cancer cells.

3. Conclusion

Curcumin-based fluorescent probes can specifically bind to a wide variety of target structures. Curcumin molecules have high electron delocalization and π-conjugated structures, with good optical and electrical properties, which can be used as fluorescent probes for the determination of biomacromolecules. In particular, the substituted groups at both ends of curcumin and its enone structures exert a great influence on the optical properties of the probe, by altering the conformation and localization of the probe and binding site as well as the characteristics of fluorescence emission wavelength and intensity.

The properties of curcumin-based fluorescent probes are summarized as below: (i) curcumin acts as a basic scaffold for the probe, and its aromatic ring structure has certain lipophilicity and BBB penetration properties; (ii) the substitution of hydroxyl and methyl groups by a strong electronic-donating group at both ends of the molecule is conducive to the red-shift emission of the fluorescent probe; and (iii) the diketone complexation with BF2 or ester groups can enhance its optical properties. In the current study, we have demonstrated that curcumin-based probes exhibit strong binding capacity and high detection efficiency for

soluble/insoluble amyloid-ß, intracranial ROS, cysteine and cancer cells.

For early AD detection, different structures of curcumin-based fluorescent probes are designed according to the target molecules. Typical molecular structure of curcumin has good detectability for insoluble Aß. The steric hindrances of curcumin scaffolds can be modified to design T-curcumin probes with better accessibility and selectivity toward soluble Aß. The chelating curcumin molecules (such as oxalate) not only enhance the optical properties of fluorescent probes but also interact with ROS, which can be used for the selective detection of ROS. The specific recognition of Cys is mostly based on Michael addition and cyclization reaction. D-A-D fluorescent probe can also be formed by adding the Olefinic double bond at both ends of the molecule, which is highly selective and sensitive to Cys. The detection of other target substances can be achieved by adding metal complexes or increasing conjugated systems for specific binding. Considering the excellent optical properties of curcumin-based fluorescent probes, the dynamic monitoring of biological macromolecules in organisms may be realized by these multifunctional curcumin-based fluorescent probes with high sensitivity, selectivity and stability in the future, which will provide a strong theoretical framework in chemistry, environmental, and bioscience sciences.

Conflicts of interest

The authors report no conflicts of interest. The authors alone are responsible for the content and writing of this article.

Acknowledgments

We are grateful to School of Pharmacy, Liaoning University for providing laboratory facilities. And we would like to express our gratitude to EditSprings (https://www.editsprings.com/) for the expert linguistic services provided. This research was financially supported by the Scientific Research Fund of Liaoning Provincial Education Department of China (No. LJC201908), and the Natural Science Foundation of Liaoning Province (No.20180510016,2019-MS-153).

REFERENCES

[1] Sato T, Hotsumi M, Makabe K, Konno H. Design, synthesis and evaluation of curcumin-based fluorescent probes to detect Aß fibrils. Bioorg Med Chem Lett 2018;28:3520–5.
[2] Zhang W H, Hu XX, Zhang XB. Dye-doped fluorescent silica nanoparticles for live cell and *in vivo* bioimaging. Nanomaterials 2016;6(5):81.
[3] Banerjee S, Chakravarty AR. Metal complexes of curcumin for cellular imaging, targeting, and photoinduced anticancer activity. Acc Chem Res 2015;48(7):2075–83.
[4] Hu L H, Shi D L, Li XM, Zhu J, Mao F, Li XK, et al. Curcumin-based polarity fluorescent probes: design strategy and biological applications. Dyes Pigment 2020;177:108320.
[5] Soleimani V, Sahebkar A, Hosseinzadeh H. Turmeric (Curcuma longa) and its major constituent (curcumin) as nontoxic and safe substances. Phytother Res 2018;32(6):985–95.
[6] Esatbeyoglu T, Huebbe P, Ernst I M, Chin D, Wagner AE, Rimbach G. Curcumin—from molecule to biological function. Angew Chem Int Ed Engl 2012;43(34):5308–32.
[7] Noorafshan A, Ashkani-Esfahani S. A review of therapeutic effects of curcumin. Curr Pharm Des 2013;19(11):2032–2046.
[8] Rahmani AH, Alsahli MA, Aly SM, Khan MA, Aldebasi Y H. Role of curcumin in disease prevention and treatment. Adv Biomed Res 2018;7.
[9] Khorasani MY, Langari H, Sany SBT, Rezayi M, Sahebkar A. The role of curcumin and its derivatives in sensory applications. Mater Sci Eng C 2019;103:109792.
[10] Satalkar V, Rusmore TA, Phillips E, Pan XL, Benassi E, Wu Q, et al. Computational modeling of curcumin-based fluorescent probe molecules. Theor Chim Acta 2019;138(2):29.
[11] Bai G, Yu C, Cheng C, Hao E, Wei Y, Mu X, et al. Syntheses and photophysical properties of BF2 complexes of curcumin analogues. Organ Biomol Chem 2014;12(10):1618–26.
[12] Felouat A, D'Aléo A, Fages F. Synthesis and photophysical properties of difluoroboron complexes of curcuminoid derivatives bearing different terminal aromatic units and a meso-aryl ring. J Org Chem 2013;78(9):4446–55.
[13] Chaicham A, Kulchat S, Tumcharern G, Tuntulani T, Tomapatanaget B. Synthesis, photophysical properties, and cyanide detection in aqueous solution of BF2-curcumin dyes. Tetrahedron 2010;66(32):6217–23.
[14] Yang J, Zhang X, Yuan P, Yang J, Xu Y, Grutzendler J, et al. Oxalate-curcumin–based probe for micro-and macroimaging of reactive oxygen species in Alzheimer's disease. Proc Natl Acad Sci 2017;114(47):12384–9.
[15] Greenhalgh R, Riley JP. The development of a reproducible spectrophotometric curcumin method for determining boron, and its application to sea water. Analyst 1962;87(1041):970–6.
[16] Lyu H, Wang D, Cai L, Wang DJ, Li XM. Synthesis, photophysical and solvatochromic properties of diacetoxyboron complexes with curcumin derivatives. Spectrochim Acta, Part A 2019;220:117126.
[17] Sherin DR, Thomas SG, Rajasekharan KN. Mechanochemical synthesis of 2, 2-difluoro-4, 6-bis (ß-styryl)-1, 3, 2-dioxaborines and their use in cyanide ion sensing. Heterocycl Commun 2015;21(6):381–5.
[18] Farooqui AA, Farooqui T. Usefulness of curcumin analogs for the diagnosis and treatment of Alzheimer sisease. In: Farooqui T, Farooqui AA, editors. Curcumin for neurological and psychiatric disorders. Academic Press; 2019. p. 231–45.
[19] Selkoe DJ, Hardy J. The amyloid hypothesis of Alzheimer's disease at 25 years. EMBO Mol Med 2016;8(6):595–608.
[20] Hardy J, Selkoe DJ. The amyloid hypothesis of Alzheimer's disease: progress and problems on the road to therapeutics. Science 2002;297(5580):353–6.
[21] Lee D, Kim SM, Kim HY, Kim YS. Fluorescence chemicals to detect insoluble and soluble amyloid-ß aggregates. ACS Chem Neurosci 2019;10(6):2647–57.
[22] Garcia-Alloza M, Borrelli LA, Rozkalne A, Hyman B T, Bacskai B J. Curcumin labels amyloid pathology *in vivo*, disrupts existing plaques, and partially restores distorted neurites in an Alzheimer mouse model. J Neurochem 2007;102(4):1095–104.
[23] Yang F, Lim GP, Begum AN, Ubeda OJ, Simmons M R, Ambegaokar S S, et al. Curcumin inhibits formation of amyloid ß oligomers and fibrils, binds plaques, and reduces amyloid *in vivo*. J Biol Chem 2005;280(7):5892–901.

[24] Chen M, Du ZY, Zheng X, Li DL, Zhou RP, Zhang K, et al. Use of curcumin in diagnosis, prevention, and treatment of Alzheimer's disease. Neural Regen Res 2018;13(4):742–752.
[25] Licha K, Olbrich C. Optical imaging in drug discovery and diagnostic applications. Adv Drug Deliv Rev 2005;57(8):1087–108.
[26] Ran C, Xu X, Raymond SB, Ferrara B J, Neal K, Bacskai B, et al. Design, synthesis, and testing of difluoroboron-derivatized curcumins as near-infrared probes for *in vivo* detection of amyloid-ß deposits. J Am Chem Soc 2009;131(42):15257–61.
[27] Yosef K, David B, Ernesto B, David S B, Joel AP, William JA, et al. Retinal amyloid pathology and proof-of-concept imaging trial in Alzheimer's disease. JCI Insight 2017;2(16):1180–6.
[28] Staderini M, Martín MA, Bolognesi ML, Menéndez JC. Imaging of ß-amyloid plaques by near infrared fluorescent tracers: a new frontier for chemical neuroscience. Chem Soc Rev 2015;44(7):1807–19.
[29] Sui Z, Salto R, Li J, Craik C, Montellano PRO. Inhibition of the HIV-1 and HIV-2 proteases by curcumin and curcumin boron complexes. Bioorg Med Chem 1993;1(6):415–22.
[30] Si G, Zhou S, Xu G, Wang J, Wu B, Zhou S. A curcumin-based NIR fluorescence probe for detection of amyloid-beta (Aß) plaques in Alzheimer's disease. Dyes Pigment 2019;163:509–15.
[31] Naiki H, Higuchi K, Hosokawa M, Takeda T . Fluorometric determination of amyloid fibrils *in vitro* using the fluorescent dye, thioflavine T_1. Anal Biochem 1989;177(2):244–9.
[32] Endo H, Nikaido Y, Nakadate M, Ise S, Konno H. Structure activity relationship study of curcumin analogues toward the amyloid-beta aggregation inhibitor. Bioorg Med Chem Lett 2014;24(24):5621–6.
[33] Du X, Wang X, Geng M. Alzheimer's disease hypothesis and related therapies. Transl Neurodegener 2018;7(1):2.
[34] Cummings J, Lee G, Ritter A, Zhong K. Alzheimer's disease drug development pipeline: 2018. Alzheimer's Dementia Transl Res Clin Interv 2018;4:195–214.
[35] Govindaraju T, Rajasekhar K, Chakrabarti M. Function and toxicity of amyloid beta and recent therapeutic interventions targeting amyloid beta in Alzheimer's disease. Chem Commun 2015;51(70):13434–50.
[36] Benilova I, Karran E, De Strooper B. The toxic Aß oligomer and Alzheimer's disease: an emperor in need of clothes. Nat Neurosci 2012;15(3):349–57.
[37] Zott B, Simon MM, Hong W, Unger F, Chen-Engerer HJ, Frosch MP, et al. A vicious cycle of ß amyloid–dependent neuronal hyperactivation. Science 2019;365(6453):559–65.
[38] Hardy J, Selkoe DJ. The amyloid hypothesis of Alzheimer's disease: progress and problems on the road to therapeutics. Science 2002;297(5580):353–6.
[39] Haass C, Selkoe DJ. Soluble protein oligomers in neurodegeneration: lessons from the Alzheimer's amyloid ß-peptide. Nat Rev Mol Cell Biol 2007;8(2):101–12.
[40] Kayed R, Canto I, Breydo L, Rasool S, Lukacsovich T, Wu J, et al. Conformation dependent monoclonal antibodies distinguish different replicating strains or conformers of prefibrillar Aß oligomerss. Mol Neurodegener 2010;5:57.
[41] Kayed R, Head E, Thompson JL, et al. Glycation stimulates amyloid formation. Sci Aging Knowl Environ 2003;300:486–9.
[42] Staderini M, Martín MA, Bolognesi ML, Menéndez JC. Imaging of ß-amyloid plaques by near infrared fluorescent tracers: a new frontier for chemical neuroscience. Chem Soc Rev 2015;44:1807–19.
[43] Ran C, Moore A. Spectral unmixing imaging of wavelength responsive fluorescent probes: an application for the real-time report of amyloid beta species in Alzheimer's disease. Mol Imag Biol 2012;14(3):293–300.
[44] Zhang X, Tian Y, Li Z, Tian X, Sun H, Liu H, et al. Design and synthesis of curcumin analogues for *in vivo* fluorescence imaging and inhibiting copper-induced cross-linking of amyloid beta species in Alzheimer's disease. J Am Chem Soc 2013;135(44):16397–409.
[45] Zhang X, Tian Y, Zhang C, Tian X, Ross AW, Moir RD, et al. Near-infrared fluorescence molecular imaging of amyloid beta species and monitoring therapy in animal models of Alzheimer's disease. Proc Natl Acad Sci USA 2015;112(31):9734–9.
[46] Li Y, Yang J, Liu H, Yang J, Du L, Feng H, et al. Tuning the stereo-hindrance of a curcumin scaffold for the selective imaging of the soluble forms of amyloid beta species. Chem Sci 2017;8(11):7710–17.
[47] Yang J, Yang J, Li Y, Xu Y, Ran C. Near-infrared fluorescence ocular imaging (NIRFOI) of Alzheimer's disease. Mol Imag Biol 2018(Suppl 1):1–9.
[48] Biancalana M, Koide S. Molecular mechanism of Thioflavin-T binding to amyloid fibrils. Biochim Et Biophys Acta Proteins Proteom 2010;1804(7):1405–12.
[49] Hamley IW. Peptide fibrillization. Angew Chem 2007;46(43):8128–47.
[50] Hanyu M, Ninomiya D, Yanagihara R, Murashima T, Miyazawa T, Yamada T. Studies on intramolecular hydrogen bonding between the pyridine nitrogen and the amide hydrogen of the peptide: synthesis and conformational analysis of tripeptides containing novel amino acids with a pyridine ring. J Pept Sci 2005;11:491.
[51] Xie H, Hou S, Jiang J, Sekutowicz M, Kelly J, Bacskai BJ. Rapid cell death is preceded by amyloid plaque-mediated oxidative stress. Proc Natl Acad Sci 2013;110:7904–9.
[52] Mclean CA, Cherny RA, Fraser FW, Fuller SJ, Smith MJ, Beyreuther K, et al. Soluble pool of Aß amyloid as a determinant of severity of neurodegeneration in Alzheimer's disease. Ann Neurol 1999;46:860–6.
[53] Lue LF, Kuo YM, Roher AE, Brachova L, Shen Y, Sue L, et al. Soluble amyloid beta peptide concentration as a predictor of synaptic change in Alzheimer's disease. Am J Pathol 1999;155(3):853–62.
[54] Condello C, Yuan P, Das P, Grutzendler J. Microglia constitute a barrier that prevents the formation of neurotoxic oligomeric beta-amyloid hot spots around plaques. Alzheimers & Dementia 2013;9(4):351.
[55] Wilkinson BL, Landreth GE. The microglial NADPH oxidase complex as a source of oxidative stress in Alzheimer's disease. J Neuroinflammation 2006;3(1):30.
[56] Bolmont T, Haiss F, Eicke D, Radde R, Mathis CA, Klunk WE, et al. Dynamics of the microglial/amyloid interaction indicate a role in plaque maintenance. J Neurosci Off J Soc Neurosci 2008;28(16):4283–92.
[57] Condello C, Yuan P, Schain A, Grutzendler J. Microglia constitute a barrier that prevents neurotoxic protofibrillar Aß42 hotspots around plaques. Nat Commun 2015;6:6176.
[58] Huang Y, Erdmann N, Peng H, Zhao Y, Zheng J. The Role of TNF related apoptosis-inducing ligand in neurodegenerative diseases. Cell Mol Immunol 2005;2(2):113–22.
[59] Wilkinson BL, Landreth GE. The microglial NADPH oxidase complex as a source of oxidative stress in Alzheimer's disease. J Neuroinflammation 2006;3:30.
[60] Li E, Kim A, Zhang L. Modeling excited states of fluorescent compounds with UV-Vis spectra calculations. J Stud Comput Chem 2007;1:1–72.
[61] Jung HS, Han JH, Pradhan T, Kim S, Lee SW, Sessler JL, et al. A cysteine-selective fluorescent probe for the cellular detection of cysteine. Biomaterials 2012;33(3):945–53.
[62] Yin J, Kwon Y, Kim D, Lee D, Kim G, Hu Y, et al. Cyanine-based fluorescent probe for highly selective

detection of glutathione in cell cultures and live mouse tissues. J Am Chem Soc 2014;136(14):5351–8.
[63] Yin K, Yu F, Zhang W, Chen L. A near-infrared ratiometric fluorescent probe for cysteine detection over glutathione indicating mitochondrial oxidative stress *in vivo*. Biosens Bioelectron 2015;74:156.
[64] Lee YH, Ren WX, Han J, Sunwoo K, Lim JY, Kim JH, et al. Highly selective two-photon imaging of cysteine in cancerous cells and tissues. Chem Commun 2015;51(76):14401.
[65] Sun Q, Sun D, Song L, Chen Z, Chen Z, Zhang W, et al. Highly selective fluorescent turn-on probe for protein thiols in biotin receptor-positive cancer cells. Anal Chem 2016;88:3400.
[66] Bu LL, Chen JQ, Wei XD, Li X, Ågren H, Xie YS. An AIE and ICT based NIR florescent probe for cysteine and homocysteine. Dyes Pigment 2017;136:724–31.
[67] Chen H, Tang Y, Ren M, Lin W. Single near-infrared fluorescent probe with high- and low-sensitivity sites for sensing different concentration ranges of biological thiols with distinct modes of fluorescence signals. Chem Sci 2016;7:1896.
[68] Liu T, Huo F, Yin C, Li J, Chao J, Zhang Y. A triphenylamine as a fluorophore and maleimide as a bonding group selective turn-on fluorescent imaging probe for thiols. Dyes Pigment 2016;128:209.
[69] Wang P, Liu J, Lv X, Liu Y, Zhao Y, Guo W. A naphthalimide-based glyoxal hydrazone for selective turn-on sensing of Cys and Hcy. Org Lett 2012;14(2):520–3.
[70] Peng R, Lin L, Wu X, Liu X, Feng X. Fluorescent sensor based on BINOL for recognition of cysteine, homocysteine, and glutathione. J Org Chem 2013;78(22):11602–5.
[71] Yuan Y, Kwok RTK, Feng G, Liang J, Geng J, Tang BJ, et al. Rational design of fluorescent light-up probes based on an AIE luminogen for targeted intracellular thiol imaging. Chem Commun 2014;50(3):295–7.
[72] Nawimanage RR, Prasai B, Hettiarachchi SU, McCarley RL. Rapid, photoinduced electron transfer-modulated, turn-on fluorescent probe for detection and cellular imaging of biologically significant thiols. Anal Chem 2014;86(24):12266–71.
[73] Miao Q, Li Q, Yuan Q, Li L, Hai Z, Liu S, et al. Discriminative fluorescence sensing of biothiols *in vitro* and in living cells. Anal Chem 2015;87(6):3460–6.
[74] Pang L, Zhou Y, Gao W, Zhang J, Song H, Wang X, et al. Curcumin-based fluorescent and colorimetric probe for detecting cysteine in living cells and zebrafish. Ind Eng Chem Res 2017;56(27):7650–5.
[75] Yue Y, Yin C, Huo F, Chao J, Zhang Y. The application of natural drug-curcumin in the detection hypochlorous acid of real sample and its bioimaging. Sens Actuators 2014;B202(10.):551–6.
[76] Rohanizadeh R, Deng Y, Verron E. Therapeutic actions of curcumin in bone disorders. Bonekey Rep 2016;5:793.
[77] Niu W, Guo L, Li Y, Shuang S, Dong C, Wong MS. Highly Selective Two-photon fluorescent probe for ratiometric sensing and imaging cysteine in mitochondria. Anal Chem 2016;88:1908.
[78] Ali F, Anila HA, Taye N, Gonnade RG, Chattopadhyay S. A fluorescent probe for specific detection of cysteine in the lipid dense region of cells. Chem Commun 2015;51:16932.
[79] Liu Y, Yu D, Ding S, Xiao Q, Guo J, Feng G. Rapid and ratiometric fluorescent detection of cysteine with high selectivity and sensitivity by a simple and readily available probe. ACS Appl Mater Interfaces 2014;6(20):17543–50.
[80] Wang L, Zhou Q, Zhu B, Yan L, Ma Z, Du B, et al. A colorimetric and fluorescent chemodosimeter for discriminative and simultaneous quantification of cysteine and homocysteine. Dyes Pigment 2012;95(2):275–9.
[81] Guo Z, Nam SW, Park S, Yoon J. A highly selective ratiometric near-infrared fluorescent cyanine sensor for cysteine with remarkable shift and its application in bioimaging. Chem Sci 2012;3:2752–60.
[82] Blondeau P, Berse RGC, Gravel D. Synthesis of some stable 7-Halo-1,4-thiazepines. potential substituted Penam precursors. Can J Chem 1971;49(23):3866–76.
[83] Chen D, Long Z, Dang Y, Chen L. A new fluorescent probe for specific detection of cysteine with facile preparation and living cell imaging. Dyes Pigm 2019;166:266–71.
[84] Chen D, Long Z, Dang Y, Chen L. A novel fluorescent probe with red emission and a large Stokes shift for selective imaging of endogenous cysteine in living cells. Analyst 2018;143:5779–84.
[85] Qi Y, Huang Y, Li B, Zeng F, Wu S. Real-time monitoring of endogenous cysteine levels *in vivo* by near-infrared turn-on fluorescent probe with large stokes shift. Anal Chem 2018;90(1):1014–20.
[86] Wasilewski M, Chojnacka K, Chacinska A. Protein trafficking at the crossroads to mitochondria. BBA Mol Cell Res 2017;1864(1):125–37.
[87] Zhang P, Guo ZQ, Yan CX, Zhu WH. Near-Infrared mitochondria-targeted fluorescent probe for cysteine based on difluoroboron curcuminoid derivatives. Chin Chem Lett 2017;28:1952–6.
[88] Wanninger S, Lorenz V, Subhan A, Edelmann FT. ChemInform abstract: metal complexes of curcumin-synthetic strategies, structures and medicinal applications. Chem Soc Rev 2015;46(36):4986–5002.
[89] Pröhl M, Schubert US, Weigand W, Gottschaldt M. Metal complexes of curcumin and curcumin derivatives for molecular imaging and anticancer therapy. Coord Chem Rev 2016;307:32–41.
[90] Zhou SS, Xue X, Wang JF, Dong Y, Jiang B, Wei D, et al. Synthesis, optical properties and biological imaging of the rare earth complexes with curcumin and pyridine. J Mater Chem 2012;22(42):22774.
[91] Lee DE, Koo H, Sun I C, Ryu JH, Kim K, Kwon IC. Multifunctional nanoparticles for multimodal imaging and theragnosis. Chem Soc Rev 2012;41:2656–72.
[92] Wang BG, König K, Halbhuber KJ. Two-photon microscopy of deep intravital tissues and its merits in clinical research. J Microsc 2010;238(1):1–20.
[93] Shan L, Xue J, Guo J, Qian J, Achilefu S, Gu Y. Improved targeting of ligand-modified adenovirus as a new near infrared fluorescence tumor imaging probe. Bioconjug Chem 2011;22(4):567–81.
[94] Albota M, Beljonne D, Brédas JL, Ehrlich JE, Fu JY, Heikal A, et al. Design of organic molecules with large two-photon absorption cross sections. Science 1998;281(5383):1653–6.
[95] Rumi M, Ehrlich JE, Heikal AA, Perry JW, Barlow S, Hu Z, et al. Structure−property relationships for two-photon absorbing chromophores: bis-donor diphenylpolyene and bis(styryl)benzene derivatives. J Am Chem Soc 2000;122:9500–7.
[96] Pi Z, Wang J, Jiang B, Cheng G, Zhou S. A curcumin-based TPA four-branched copper(II) complex probe for *in vivo* early tumor detection. Mater Sci Eng C 2015;46:565–71.
[97] Xu GY, Wang JF, Liu T, Wang MH, Zhou SS, Wu BX, et al. Synthesis and crystal structure of a novel copper complex of curcumin-type and its application in and imaging. J Mater Chem B 2014;2(23):3659–66.
[98] Harding JL. Composite materials with embedded metal organic framework catalysts for nitric oxide release from bioavailable S-nitrosothiols. J Mater Chem B 2014;2(17):2530–6.
[99] Xu G, Wang J, Si G, Wang M, Wu B, Zhou S. Two-photon absorption and cell imging of two multi-branched dyes based on curcumin. Dyes Pigment 2015;123:267–73.